Compressible Ionized Natural 3D Interconnected Loofah Membrane for Salinity Gradient Power Generation

Pengcheng Luan, Yuyue Zhao, Qiang Li, Daxian Cao, Ying Wang, Xiao Sun, Chao Liu, and Hongli Zhu*

Large-scale salinity gradient power energy harvesting has generated broad attention in recent years, in which affordable ion-selective membranes (ISMs) are essential for its practical implementation. In this study, for the first time, ISMs derived from natural loofah sponge are reported, which have features of high hydrophilicity, superior ion conductivity, and 3D interconnected long fibers. The permselectivity and ion conductivity of loofah-based anion-selective membranes (ASMs) and cation-selective membranes (CSMs) are designed by chemical modification of the surface functional groups of loofah fibers and followed with compression and the resin filling. The charged nanochannels inside the ISMs are served as ion conductive and selective channels based on the nanofluidic effects and Donnan exclusion. Meanwhile, the unique isotropic structure endows excellent dimensional stability under the NaCl solution for months. When ISMs are used for salinity gradient power generation from the gradient of artificial seawater and river water, the maximum power density is 18.3 mW m^{-2}. When ten units of loofah-based ISMs are stacked in series, a voltage as high as 1.55 V is achieved. The results highlight the great potential of natural fibers for fabricating affordable, durable, and high performance ISMs, paving a sustainable pathway for developing high-performance, durable, and low-cost salinity gradient power generators.

1. Introduction

Electricity generated from fossil fuels has dominated current energy supply chains. Globally, over 64% of electricity is generated by burning fossil fuels.[1] Although fossil energy has brought great convenience to our lives, it is nonrenewable and associated with severe environmental concerns, such as polluting air, water, and soil. The combustion of fossil fuel for electricity generation has significantly contributed to the worldwide air pollution, the diseases caused by which results in about 6.5 million deaths per year.[2] Meanwhile, electricity generation from fossil fuels is also one of the main sources of greenhouse gas, exceeding the total emissions of transportation.[3]

P. Luan, Y. Zhao, Q. Li, D. Cao, Y. Wang, X. Sun, C. Liu, H. Zhu
Department of Mechanical and Industrial Engineering
Northeastern University
360 Huntington Avenue, Boston, MA 02115, United States
E-mail: h.zhu@neu.edu

Regarding the sustainable development of our society, clean and renewable energy harvesting with minimum environmental impacts represents an emerging need.

Several renewable energy resources have been sought after as the alternatives to fossil energy in recent decades, such as solar, wind, biofuel, tides, geothermal heat, and so on.[4] Among them, salinity gradient energy generated from mixing the river water and seawater is recognized as a promising renewable power source with low environmental impact and high energy reservation.[5,6] The main mechanism of salinity gradient energy generation is to convert the entropy produced by mixing two solutions at different concentrations into electrical energy and then harvest it. The main byproduct is the saltwater used during the process, suggesting the environmental friendliness of the salinity gradient energy. The power from the discharge of river water into seawater was estimated at a range of 1.4–2.6 TW, corresponding to the output of about 2000 nuclear power plants that can fulfill 80% of the global energy demand.[7,8] In the implementation of the salinity gradient energy harvesting, several technologies have been used to harvest the salinity power, including reverse electrodialysis (RED),[9] pressure retarded osmosis (PRO),[10] and capacitive mixing.[11] Among them, membrane-based technologies (PRO and RED) feature high power densities.[12] As compared to PRO, the RED has the advantage of fewer membrane fouling problems. Although PRO typically has higher power densities at the starting age of the electrical generation, membrane fouling is listed as one of the major challenges for the commercialization of PRO, which can cause an undesirable decrease in power densities and water flux.[13] The fouling issue of RED is less sensitive than PRO due to their fundamentally different mechanisms. In RED, instead of relying on water transport through semi-permeable membranes to generate electricity, electricity difference is generated by the migration of cations (Na$^+$) or anions (Cl$^-$) through cation-selective membranes (CSMs) or anion-selective membranes (ASMs) from high salinity to low salinity.[14] RED relies on ion transport through ion-selective membranes (ISMs) and continuous water flows along the membrane, resulting in a less pronounced fouling issue than PRO.[15] Therefore, RED is recognized as one of the

ADVANCED
SCIENCE NEWS
www.advancedsciencenews.com

NANO · MICRO
small
www.small-journal.com

most emerging membrane technologies for salinity gradient power generation with pilot-scale application prospects.[7] However, current challenge in the large-scale application of RED remains in the relatively low power densities and efficiencies as well as the high cost of ISMs.[16] For instance, the prices of commercialized ASM (AMI-70001S) and CSM (CMI-7000S) are ≈$290 m^{-2}.[17] Therefore, developing affordable, scalable, and high-performance ISMs has a practical significance in RED power generation.

Loofah sponge, the vascular bundle of mature luffa cylindrical, is a natural material consisting of a fibrous interconnected network with a multichannel hollow structure.[18] Recent researches have proved that the loofah sponge fibers have high mechanical strength,[19] versatile surface chemistry,[20] high hydrophilicity,[21,22] and antibacterial properties.[23] Besides, it is well known that the permselectivity (the selectivity towards the transport of ions with the opposite charge) of ISMs increases as the increment in ion transport length.[24] Loofah sponge fibers are generally very long, twisted, and interconnected, which thus is promising for fabricating highly permselective ISMs with long ion transport paths. Based on these merits, in this study, for the first time, we used a loofah sponge to fabricate durable and high-performance heterogeneous ASMs and CSMs and applied them in the RED. However, some disadvantages could limit this application. For example, loofah sponge has a weak surface charge, low fiber density, and high pore volume that could decrease the permselectivity and ion conductivity. We therefore did chemical modifications to improve the surface charges, compressed the loofah sponge to increase the fiber density and decrease the voids, filled the compressed loofah with epoxy resin to enhance selectivity, and finally polished the loofah membrane to expose its fibers for ion transport. The obtained ASMs and CSMs exhibited excellent ion conductivity, high permselectivity, and superior durability. During the conversion of the salinity into electricity, loofah-based REDs showed high power density and energy conversion efficiency. Combining its low cost and facile fabrication process, the loofah-based ISMs derived from Nature pave the way for constructing affordable, scalable, and durable ISMs for salinity gradient power harvesting.

2. Results and Discussions

Loofah (**Figure 1**a) as a vegetable source has been widely planted in tropical regions. Loofah harvested at an early stage is edible, but fully ripened loofah is fibrous. The ripen loofah with the sponge structure contains hoop walls and core parts (Figure S1a, Supporting Information). All these parts are comprised of fiber with a highly porous structure (Figure S1a, Supporting Information) but good mechanical strength.[19] Moreover, loofah is antibacterial and super-hydrophilic, making it widely used as scrubbing sponges for dishwashing and cleaning. Based on these unique features, in this study, we used loofah to make membranes for both ASMs and CSMs, in which the interconnected networks, super-hydrophilicity, dimensional stability in the aqueous solution, and mechanical robustness of loofah play essential roles. As shown in Figure S1a,S1b, Supporting Information, we removed the loofah's core part and used the hoop walls to process loofah into the membrane. Even though natural loofah itself has abundant hydroxyl groups resulting in negative surface charges, the charge is limited.
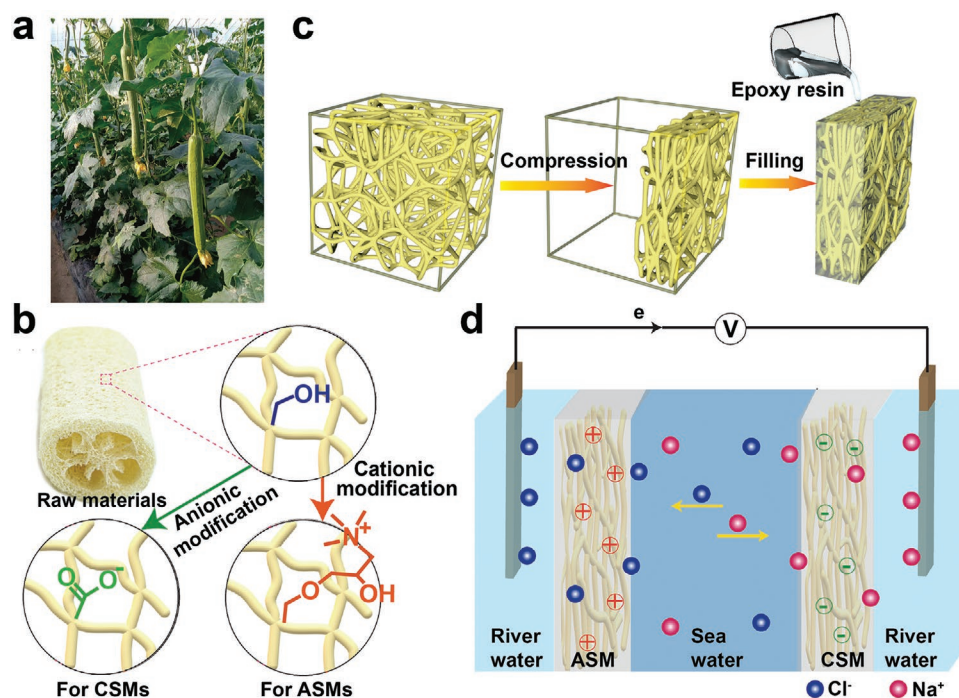

Figure 1. Schematic illustration of using loofah for the salinity gradient power generation. a) Natural growth of *Luffa cylindrica*. b) Ionic modification of loofah sponge for CSMs and ASMs. c) Loofah-based ISMs fabrication by compression and resin filling. d) Configuration of salinity gradient power generation device with loofah-based ASM and CSM as essential ISMs.

ADVANCED
SCIENCE NEWS
www.advancedsciencenews.com

NANO · MICRO
small
www.small-journal.com

Therefore, in this work, we developed a strategy to enhance its negative charges by converting its surface hydroxyl groups into more negatively charged carboxyl groups and used them as CSMs (Figure 1b and Figure S1c, Supporting Information). On the other hand, loofah must have substantial positive surface charges to be applied as ASMs; thus, we grafted quaternary ammoniums to loofah to make it positively charged (Figure 1b and Figure S1c, Supporting Information).

After the chemical modification of surface charges, loofah was compressed, filled with resin (Figure 1c, Figure S1d,S1e, Supporting Information), and then polished (Figure S1f, Supporting Information). Compression can efficiently increase the fiber density and decrease the voids of the loofah. Since the ions were transported by the loofah fiber (Figure S2, Supporting Information), the ion transport paths per unit volume were increased after compression, which can enhance ion conductivity and permselectivity. Macropores and voids remained after the compression was filled with resin to avoid a direct mix of electrolytes and enhance selectivity. Polishing was performed afterward to expose the loofah fibers from the excess resin for ion transport. After the abovementioned modifications, the resultant loofah-based ISMs (ASMs and CSMs) exhibit uniform surfaces (Figure S3, Supporting Information) and a much higher ion conductivity and permselectivity than non-treated ISMs. As illustrated in Figure 1d, when the loofah-based ISMs were used in the RED, the ASMs and CSMs could selectively transport cations (Na^+) and anions (Cl^-) from high salinity to low salinity, which created an electrical potential difference and therefore converted salinity gradient energy directly into electricity.

Compared with other abundant lignocellulosic biomass matrixes such as wood, bamboo, grass, and agricultural wastes, loofah possesses several exceptional advantages, including 3D interconnected multichannel structure, high hydrophilicity, and excellent compressibility (**Figure 2**a). All these unique characteristics of loofah make it a promising candidate for ISMs.

Loofah exhibits a 3D interconnected multichannel structure, which not only has good mechanical strength and dimensional stability under aqueous conditions, but also provides a variety of extended ion transport paths (Figure 2b_1,2b_2). Compared to that of other lignocellulosic biomass (e.g., wood)-based ISMs with short directional ion transport paths,[17] this extended ion transport path could result in a higher permselectivity of resultant ISMs. Uniquely, for each single fiber in loofah, numerous multichannels at micro- to nano- scale are highly aligned. As shown in Figure 2b_3, 2b_4, 2b_5, 2c, hollow microchannels with a diameter of ≈10–20 μm and a wall thickness of ≈100–200 nm were aligned along with the loofah fibers. These loofah fibers contain abundant aligned and hydrophilic nanocellulose (Figure 2b_6). All these aligned nanofibrils allow ions to be transferred directionally along the fiber walls. Moreover, according to the nanofluidic effects,[25,26] when these nanofibrils are strongly charged, these nanofibrils could enable the resultant ISMs with excellent ion transport behavior in terms of high ion conductivity and permselectivity.[17]

Loofah is highly hydrophilic. The hydrophilicity is critical in improving ion conductivity.[27] The most developed lignocellulosic biomass-based ISM is wood, which normally has relatively weaker hydrophilicity due to its relatively high content of hydrophobic lignin (20–30 wt.%) and low content of

hydrophilic polysaccharides (40–45 wt.% cellulose and 20–30 wt.% hemicellulose).[28] This weak hydrophilicity could induce low membrane conductivity and thus limits the power output when it is used in the RED.[27] In contrast, loofah contains a much higher content of hydrophilic cellulose (≈60 wt.%) and hemicellulose (≈30 wt.%) along with a much lower content of lignin (≈10 wt.%),[29] which makes it have much-enhanced hydrophilicity. The ratio of lignin-to-polysaccharides (cellulose and hemicellulose) has been used to determine the hydrophilicity of lignocellulosic biomass.[30] As calculated from the compositions mentioned above, this lignin-to-polysaccharides ratio for loofah is at ≈9.0, which is much higher than that of wood (≈2.0–3.8). Together with the highly porous and multichannel structure, this high hydrophilicity endows loofah with a superior water adsorption capability. As shown in Figure 2d, loofah exhibited water adsorption (**Equation (1)**) of 2.41 g g^{-1}, which was higher than that of basswood (1.31 g g^{-1}), proving the high water absorption capacity of loofah.

Loofah has excellent compressibility. Compression has been widely used to reduce the pore volume of lignocellulosic biomass and thus significantly increase its fiber density.[31] The fibers on both surfaces (Figure 2e_1,2f_1) and cross-section (Figure 2e_2,2f_2) became much denser after being compressed. The densified loofah could have more fibers to participate in ion transport in a unit volume (Figure 2g). Besides, after compressing, the 3D interconnected structure of the loofah can be maintained, resulting in longer ion transport paths in a unit volume and promote the permselectivity compared to the relatively straight paths before compressing (Figure S4, Supporting Information). In fact, the thickness of fully compressed loofah decreased by ≈80–90% after hot compressing, associating with significant decreases in the pore volume from 3.93 to 0.48 cm^3 g^{-1} and the fiber density increases from 0.11 to 0.86 g cm^{-3}, which can thus much increase the ion conductivity and permselectivity of the resultant ISMs. Overall, the resultant loofah with high fiber density, 3D interconnected multichannel structure, and high hydrophilicity is a promising matrix for fabricating high-performance and durable ISMs.

In order to utilize loofah for ASMs and CSMs, the surface charges of the loofah were modified to enable its high permselectivity. As for loofah-based ASMs, we grafted quaternary ammoniums to loofah to make it surface positively charged. As shown in **Figure 3**a, the C6 primary hydroxyl groups in some of the anhydroglucose units of cellulose were in situ substituted by cationic 3-(trimethylammonium)propyl groups by the etherification reaction. 3-chloro-2-hydroxypropyl triethyl ammonium chloride as a reactant first loses its hydrogen chloride under alkaline conditions to form glycidyl triethyl ammonium chloride, which then reacts with the hydroxyl group of cellulose through an esterification reaction.[32] Fourier-transform infrared spectroscopy (FTIR) was used to characterize the surface functional groups of modified loofah fibers. As presented in Figure 3b and Figure S5, Supporting Information, two new peaks at 1043 and 1611 cm^{-1} assigned to the C−N and N−H stretching vibration respectively,[17,33] can be found for positively charged loofah (P-loofah), indicating the successful etherification of loofah after the cationic modification.

As for loofah-based CSMs, the hydroxyl groups were in situ oxidized into more negatively charged carboxyls by the
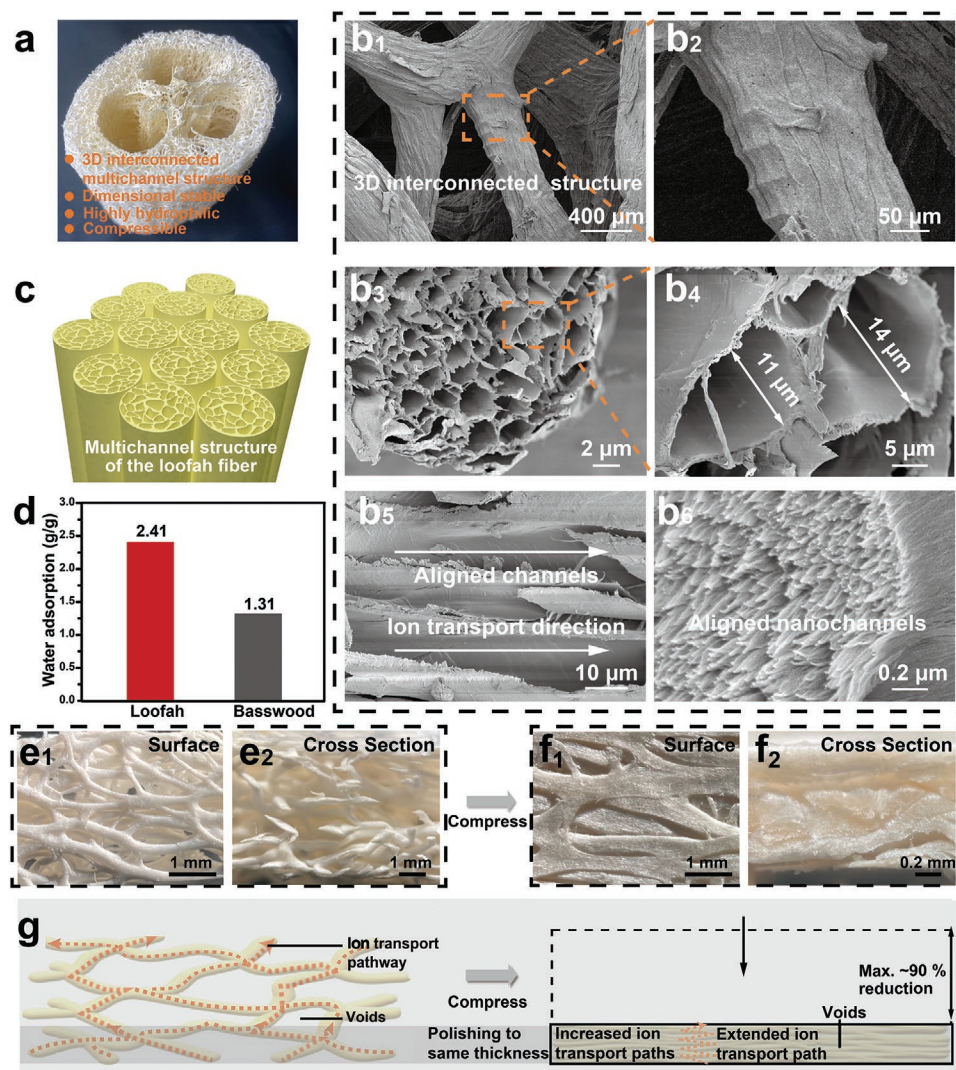
**ADVANCED
SCIENCE NEWS**

www.advancedsciencenews.com

NANO · MICRO

small

www.small-journal.com

Figure 2. Loofah as a promising natural material for fabricating low-cost and high-performance ISMs. a) Photograph of natural loofah. b_1) SEM image of the 3D interconnected structure of the loofah. b_2) Magnified SEM image of the loofah fiber in b_1. b_3) SEM image of the multichannel structure inside a single loofah fiber. b_4) Magnified SEM image of the microchannel with a diameter of ≈10–20 μm. b_5) SEM image showing aligned channels inside the loofah fiber. b_6) SEM image showing aligned nanochannels composed with cellulose nanofibrils. c) Schematic illustration of multichannel structure of the loofah fiber. d) Comparison of water adsorption of loofah and basswood. Optical microscope photos of the natural loofah from e_1) surface section and e_2) cross-section with high pore volume and low fiber density. Optical microscope photos of the compressed loofah from f_1) surface section and f_2) cross-section with decreased pore volume and increased fiber density. g) Schematic illustration of ion transport behavior of loofah before and after compression.

(2,2,6,6-tetramethylpiperidine 1-oxy radical (TEMPO)) mediated oxidation (Figure 3a). TEMPO served as the catalyst was first oxidized by the NaClO to TEMPO+, which could subsequently oxidize primary hydroxyl groups of surface cellulose to carboxyl groups.[34] In Figure 3b and Figure S5, Supporting Information, the new adsorption bands at 1600 and 1720 cm^{-1} assigned to the C=O stretching of carboxylate (−COO$^-$) and free carboxyl groups (−COOH),[34] respectively, can be found for negatively charged loofah (N-loofah), which evidenced the conversion of hydroxyls in the loofah to carboxyl groups by TEMPO-mediated oxidation.

Zeta potential test was further used to evaluate the cationic and anionic modifications of loofah. The zeta potential of raw loofah was at −11.4 mV, which shifted to 29.6 mV after

cationic modification and −34.4 mV after anionic modification (Figure 3c). Furthermore, since salt concentration is an important factor that affects the surface charge density by compressing the electric double layer (EDL) on the charged surface, the Zeta potential at different NaCl concentrations was also tested. As shown in Figure 3d, increasing the salt concentration slightly reduced the surface charge of both N-loofah and P-loofah implying high charge stability even in a high NaCl concentration as high as 1.0 mol L^{-1}. Meanwhile, the electrolyte pH significantly impact the Zeta potential of the membrane by affecting the ionization of the charged surfaces. The absolute value of Zeta potential is reduced through suppressing the surface ionization by decreasing the pH in the case of N-loofah or by increasing the pH in the case of P-loofah (Figure 3e).
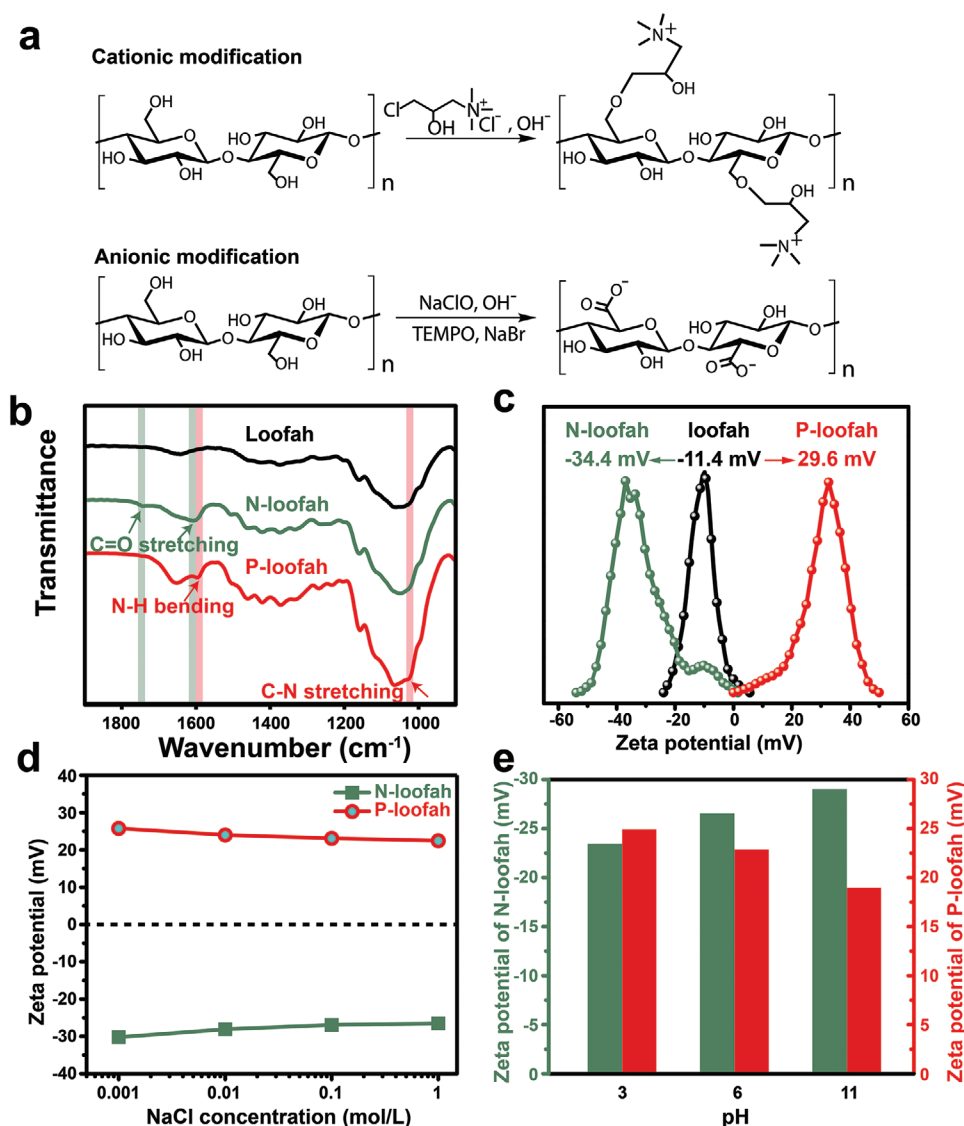
Figure 3. Chemical modification and characterization of P-loofah and N-loofah. a) In situ modification of loofah via etherification reaction for cationic modification (P-loofah) and TEMPO-mediated oxidation for anionic modification (N-loofah) during fiber modifications. b) FTIR spectra of loofah, N-loofah, and P-loofah. c) Zeta potentials of loofah, N-loofah, and P-loofah at the concentration of 0.1 mg mL^{-1} diluted by deionized water. d) Zeta potentials of loofah, N-loofah, and P-loofah at different NaCl concentrations (≈0.001–0.1 M NaCl). e) Zeta potentials of loofah, N-loofah, and P-loofah in 0.1 M NaCl at different pH (≈3–11).

Moreover, surface charge density strongly affects the ion transport behavior in the loofah fiber and impacts the permselectivity and ionic conductivity of the resultant loofah-based ISMs.[27] By using the Grahame equation (**Equations (1)** and (**3**)) the surface charge density can be calculated from the above zeta potential data, which are at −2.17 and 1.86 mC m^{-2} for N-loofah and P-loofah in 0.001 M NaCl solution, respectively. The absolute values of these surface charge density data were much higher than that of raw loofah (−0.73 mC m^{-2}), highlighting a significant increase in the surface charge of loofah after the ionic modifications. Overall, the ASMs and CSMs with largely improved surface charge density could be pH-sensitive and high salt stable.

In order to investigate the ion transfer channels of the loofah-based ISMs, a laser scanning confocal microscope

(LSCM) was used. As shown in **Figure** 4a$_1$–a$_6$, the loofah fibers as the efficient ion transport channels were clearly observed at different depths. Combining the 3D reconstruction technology (Figure 4b), we observed that the loofah fibers were densely packed after compression and its interconnected multichannel structure was fully maintained after resin filling and polishing (Figure 4c,d). Additionally, no apparent bubbles and defects have been found in the ISMs, implying the resin is fully filled into the macropores and voids of the loofah. Moreover, we measured the pore size distribution of our loofah-base ISMs by a volumetric adsorption analyzer to further investigate the filling completeness of the resin and evaluate the effective size of ion selective channels. Figure S6, Supporting Information, showed the pore size of our ISMs is
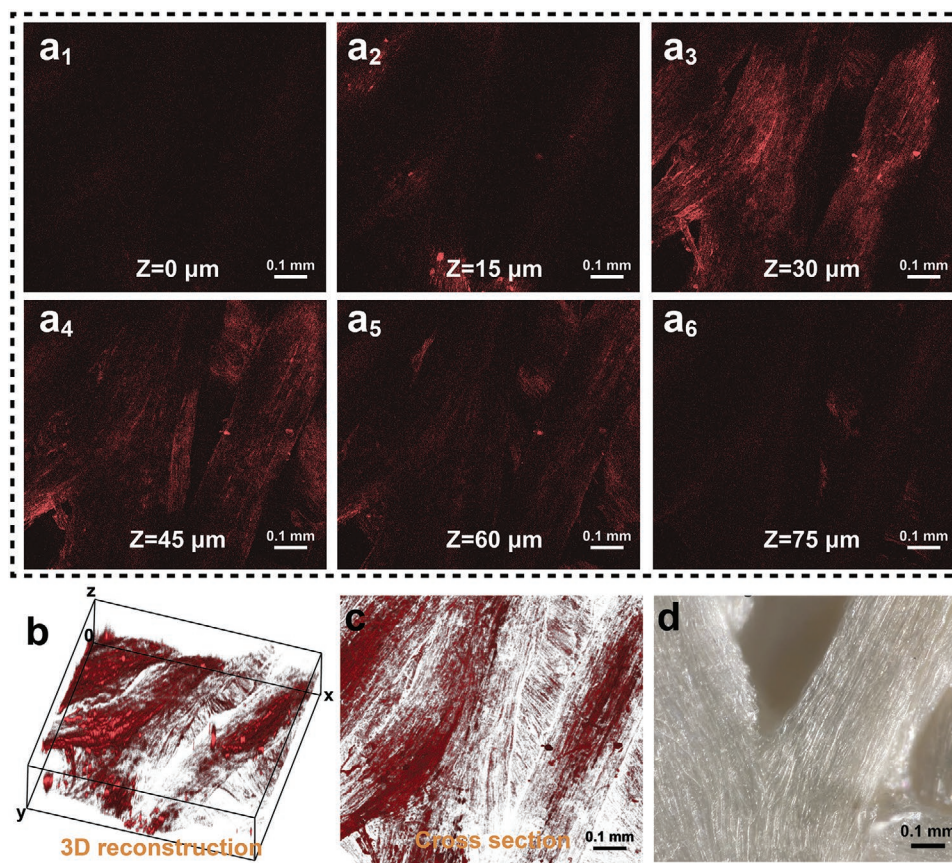
ADVANCED
SCIENCE NEWS

www.advancedsciencenews.com

NANO · MICRO
small
www.small-journal.com

Figure 4. a) LSCM images of loofah-based ASM at different depths: 0, 15, 30, 45, 60, and 75 µm. b) 3D reconstruction of loofah-based ASM. c) Cross-section image of densely packed loofah embedded in the epoxy resin. d) Optical microscope photograph of compressed loofah membrane without resin filling.

ranging from 34.3 to 63.4 Å, and the calculated average pore size of 41.3 Å.

The charged nanochannels served as efficient ion conductive and selective channels after chemical modification due to the nanofluidic effects and Donnan exclusion. The ion transport behaviors of ASMs and CSMs were illustrated in **Figure 5**a. In the loofah-based ASMs and CSMs, counter-ions could be transported in the charged nanochannels of the loofah fibers. The surface functional groups ($-COO^-$ for CSMs and $-NH_4^+$ for ASMs) could promote the effective attraction of the counter-ions and repulsion of co-ions due to the electrostatic interaction. Moreover, according to the nanofluidic effects, in the charged nano-channels structures of the loofah, the ions were transported via the EDL at its solid-liquid interface, which followed the surface-charge-governed ionic conductance, thereby increasing its ion permselectivity.[35]

In order to investigate the ion transport performances of the prepared loofah-based ISMs and the effects of loofah compression on the ion transport behaviors, water adsorption, permselectivity, and ion conductivity were further characterized. Besides, to investigate the effects of loofah structure and water adsorption capability on the ion transport behaviors, home-made wood ISMs with low water adsorption capability and short ion transport paths were used as a control sample. The water content plays a crucial role in the ion transport

properties of ISMs because water molecules can be served as the medium to promote ion transport in the ISMs. In the case of high water content, the extra swelling of the ISMs would loosen the membrane structures, resulting in the decrease of surface charge density. The loose membrane could promote ion conduction through the membrane but was detrimental to membrane permselectivity.[27] In addition, the compressibility of loofah-based membrane strongly impacted water adsorption. The water adsorption of loofah-based ISMs with different compression degrees was investigated in Figure 5b. The fully compressed ISMs exhibited much higher water adsorption (0.323 g g^{-1}) than medium compressed (0.101g g^{-1}, with a thickness decrease of 42% after compression) and non-compressed ISMs (0.028 g g^{-1}) due to the increased fiber density.

In addition, ion conductivity and permselectivity are two of the most important parameters that can determine the general power output of the RED. To investigate the ion conductivity of as-prepared ASMs and CSMs, the membrane resistance was measured by electrochemical impedance spectroscopy (EIS), and the results are shown in Figure 5c. After soaking in 0.001 M NaCl solution for 24h, the ion conductivities of fully compressed ASM and CSM calculated by **Equation (4)** were 0.543 mS cm^{-1} for ASM and 0.620 mS cm^{-1} for CSM, respectively, which were a lot higher than medium compressed (0.101 mS cm^{-1} for ASM and 0.123 mS cm^{-1} for CSM) and non-compressed
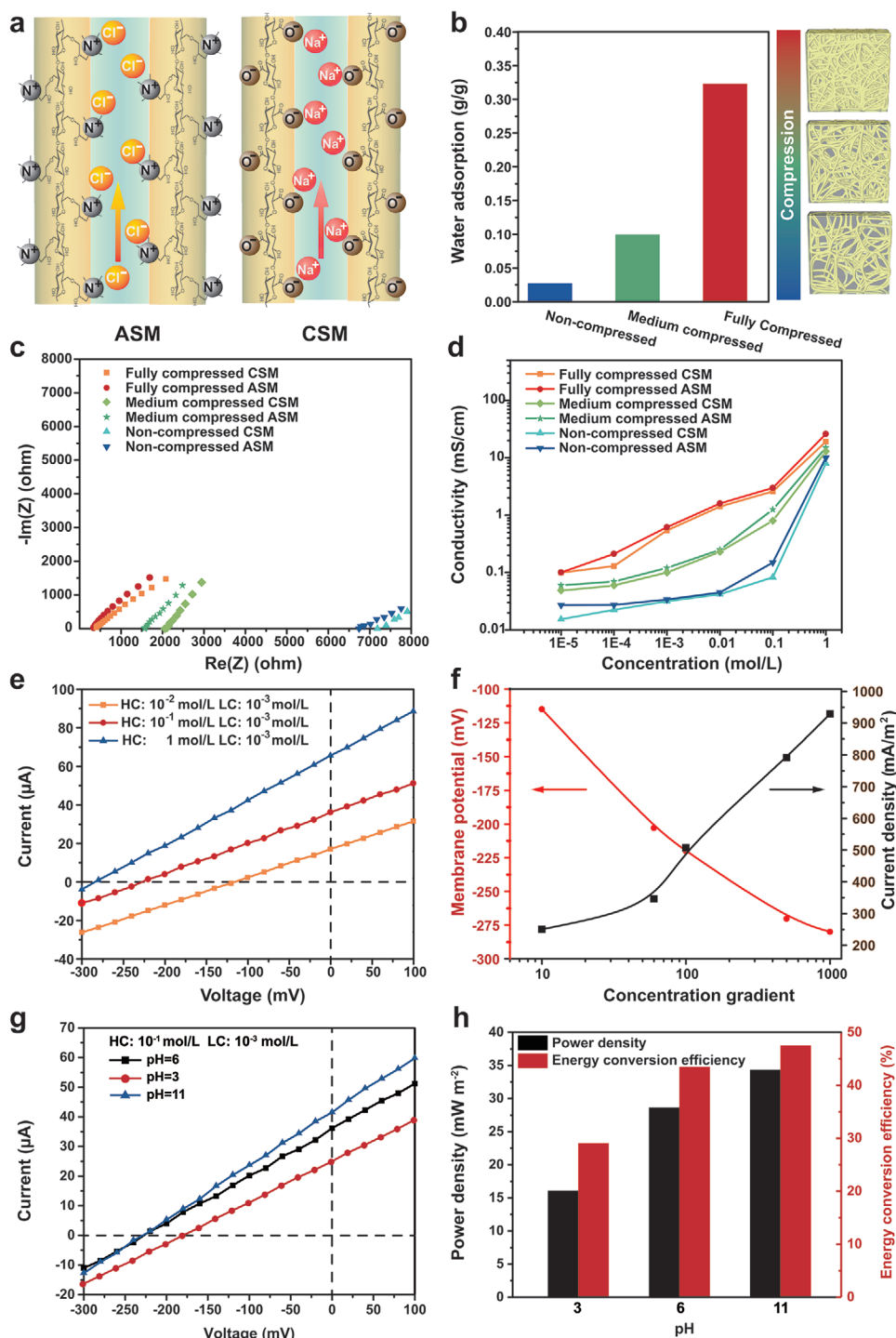
Figure 5. a) Schematic illustration of ion-selective transport along the nanochannels in the ASM (left) and CSM (right). b) Water adsorption of non-compressed, medium compressed, and fully compressed loofah-based ISMs. c) EIS curves of compressed CSM and ASM with a dimension of 3.8 mm by 3.8 mm by 0.3 mm. d) Ion conductivity curves of different as-prepared CSMs and ASMs at different concentration NaCl electrolytes. e) Current-voltage curves of home-made RED assembled by CSM, ASM, and rubber barrier, in which high concentration NaCl solution was in the middle reservoir (1, 0.1, or 0.01 м) and low concentration NaCl solution (0.001 м) was in the neighbor reservoir. f) The membrane potential and current density with the CSM and ASM at different concentration gradients. g) Current-voltage curves of loofah-based RED at different pH and h) the related power density and comparable energy conversion efficiency.

ASM and CSM (0.031 mS cm^{-1} for ASM and 0.034 mS cm^{-1} for CSM). These results confirmed that the compression process improves the ion conductivity of loofah-based ISMs by increasing the fiber density.

**ADVANCED
SCIENCE NEWS**
www.advancedsciencenews.com

NANO · MICRO
small
www.small-journal.com

To further evaluate the effect of supporting electrolyte concentration on the ion transport properties of loofah-based ISMs, the ion conductivity at different concentrations of NaCl solutions was investigated. As shown in Figure 5d, when the salt concentration was less than 0.01 m, the ion conductivity of both ASM and CSM increased slowly with the NaCl concentration increasing. As the NaCl concentration was above 0.01 m, the ion conductivity of both ASMs and CSMs increased nearly proportional with the NaCl concentration increasing. This indicated that the ion transport process at low concentration NaCl solutions was determined by the surface-charge-governed transport, which was the nanofluidic effects feature.[35] Additionally, the fully compressed ISMs showed a lot higher ion conductivity than medium compressed ISMs, and non-compressed ISMs, especially at low NaCl solutions. As compared to the homemade wood-based ISMs, owing to the high water adsorption, the compressed ISMs also exhibited higher ion conductivity (≈12 times higher than wood membrane at 0.01 m NaCl, Figure S7, Supporting Information). Overall, the compressed loofah-based ASMs and CSMs showed excellent ion conductivity, indicating that increasing fiber density was an efficient way to increase the ion conductivity of lignocellulosic biomass with loose and porous structures.

As one of the critical properties, the permselectivity of ISMs indicates their capacities to selectively transport counter-ions and repel co-ions.[35] The enhancement of ISMs permselectivity generally can result in an increase in the power output and energy conversion efficiency.[27] According to **Equation (5)**, the permselectivity of ISMs can be obtained by calculating the ratio of the measured membrane potential to the theoretical membrane potential under a certain salinity gradient. The permselectivity of our compressed CSMs and ASMs was measured by a home-made RED device using Ag/AgCl plate as the electrode (Figures S8 and S9, Supporting Information). The RED device consisted of three reservoirs and was separated by compressed ASM and CSM with an effective area of 60 mm^2 and a membrane distance of 1.5 mm.

The low concentration of NaCl solution (0.001 m) was filled in the side reservoirs, and the higher concentration of NaCl solution (1, 0.1, or 0.01 m) was filled in the middle reservoir. Figure 5e showed the typical linear voltage-current curves at different concentration gradients (1000, 100, and 10). When the salinity gradient was at the range of 10–1000, the absolute value of membrane potentials and current densities (equal to the short circuit current divided by the effective membrane area) increased with the increase of the salinity gradient (shown in Figure 5f). The calculated permselectivities of our REDs at the concentration gradients of 10 and 100 were as high as 97.4% and 95.3%, and the energy conversion efficiencies calculated by **Equation (7)** were as high as 47.4% and 45.4% (Table S1, Supporting Information). The high permselectivity and conversion efficiency of our compressed loofah-based RED is attributed to its nano-sized channels (averaged diameter of 41.3 Å, Figure S6, Supporting Information) and extended ion transport paths after compression (Figure 2g). These results showed great potential for harvesting salinity gradient energy by mixing river water and seawater (normally with a concentration gradient of 60). In addition, the obtained high current densities agreed with the aforementioned high ion conductivity of our loofah-based

ISMs. Therefore, despite the high ion conductivity, compressed ASMs and CSMs also exhibited a high permselectivity, especially when at a low salinity gradient (≈10–100). These results can be attributed to the increase of charge and fiber densities. Compared with non-compressed ISMs, the co-ions were harder to transport along the nanochannels of extended loofah fibers and migrate through the ISMs owing to the high content of charged groups and long ion transport paths. The heterogeneous ISMs-based RED with our high ion-selective and ion-conductive membranes could obtain high power densities of 8.2 and 33.8 mW m^{-2} at concentration gradients of 10 and 100 (**Equations (8)** and **(9)** and Table S1, Supporting Information). Although the power density of the heterogeneous loofah-based RED is lower than the recently reported homogeneous REDs due to the use of non-ionic conductive epoxy resin as the filler, it is cost-effective and shows better power densities and energy conversion efficiencies than other low-priced heterogeneous lignocellulosic biomass-based REDs,[17] making it promising for large-scale salinity energy harvesting.

The pH of electrolytes could affect the dissociation of functional groups (−COOH and -R$_4$NCl) on ISMs, which plays a very crucial role in ion conduction. The effect of electrolyte pH on current-voltage (I-V) response was investigated and shown in Figure 5g. With the pH varying from 3 to 11, the total RED energy output increased from 16.1 to 34.4 mW m^{-2}, and the energy conversion efficiency increased from 29.1% to 47.5% (Figure 5h). These results could be mainly attributed to the different dissociation states of the cation and anion functional groups in different pH electrolytes. The carboxylate groups (–COO$^-$) tended to be protonated to form carboxyl groups (–COOH) in the acidic atmosphere (pH = 3), attributing to Le Chatelier's principle. When the pH of the electrolyte increased from 3 to 11, the carboxyl groups (−COOH) tended to be deprotonated to form the cation-selective groups (−COO$^-$), which was favorable to improve ion-selective capacity. On the other hand, the anion functional groups (−R$_4$NCl) showed less effect in the electrolytes with various pHs because they can be completely dissociated to form the anion-selective groups (−R$_4$N$^+$) even under the alkaline condition. In addition, although increasing the pH reduces the absolute value of the zeta potential of ASM slightly reducing its selectivity, it increases the absolute value of the zeta of CSM, which is beneficial to increase its selectivity. Moreover, pH changes affect the zeta potential of ISM, which in turn affects its permselectivity and energy conversion efficiency. Increasing pH could slightly reduce the permeselectivity of ASM by reducing its absolute value of zeta potential, but it increases the permselectivity of CSM by increasing its absolute value of zeta potential as well as cation-selective groups. As a result, enhanced power density and energy conversion efficiency were obtained. Moreover, the different ion-selective behavior of CSMs and ASMs at acidic and alkaline atmospheres indicated the loofah-based RED is a pH-responsive device.

The electrical power generation properties by converting salinity-gradient between seawater and river water were investigated in **Figure 6**. The 0.01 and 0.6 m NaCl solutions were employed to simulate the river water and seawater, respectively. The RED was prepared with one unit and filled with the "seawater" in the middle reservoir and the "river water" in the reservoirs on the side (Figure S8a,b and Figure S9,
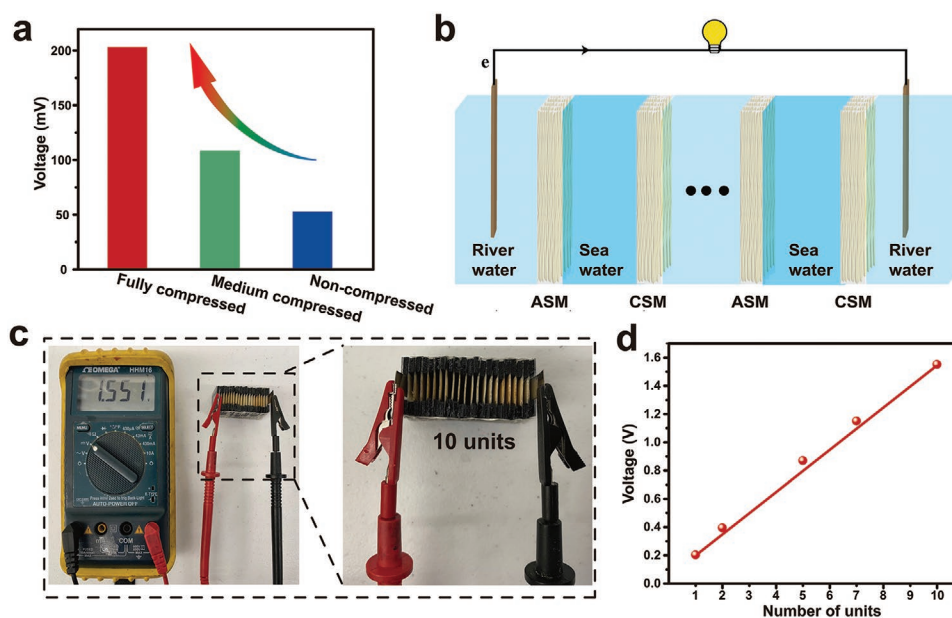
Figure 6. a) Output voltage of non-compressed, medium compressed, and fully compressed ISMs-based RED. b) Schematic illustration of the tandem RED. c) 10 tandem RED outputs a voltage as high as 1.551 V under the concentration gradient of 60 (0.01 M NaCl solution as the artificial river water and 0.6 M NaCl solution as the simulated seawater). d) A good linear relationship of voltage as the increase of the RED unit under the concentration gradient of 60 (0.01 M NaCl solution as the simulated river water and 0.6 M NaCl solution as the simulated seawater).

Supporting Information). The maximum output voltage of one RED unit with loofah-based ASM and CSM reached 203.3 mV (Figure 6a), which was 2.85-fold higher than that of the RED with a non-compressed loofah (52.7 mV, Figure 6a). The calculated permeselectivity of fully compressed, medium compressed, and non-compressed loofah-based RED were 96.8%, 51.6%, and 25.1%, respectively. These results confirmed that the compression increased the permselectivity of loofah-based ISMs. During salinity energy conversion, the generated power density and energy conversion efficiency of the compressed loofah-based ISM reached up to 18.3 mW m^{-2} and 46.8%, respectively (Table S2, Supporting Information).

Moreover, when in series (Figure S8c, Supporting Information), voltages can be significantly increased as the units stacked. Figure 6b illustrated the tandem REDs consisting of alternating compressed ASMs and CSMs. In Figure 6c, the maximum output voltage of 10 units reached up to 1.511 V. Besides, a good linear relationship between the number of units and the maximum output voltage was observed in Figure 6d, where each unit cell can generate an output voltage of ≈150–200 mV. The voltage of RED slightly decreased with time going after it reached the maximum value, which was attributed to the decrease of salinity gradient as the selective ion transportation. In practice, continuous flow of river water and seawater are adopted to maintain the concentration gradient, so that RED can continuously supply high power output. Overall, during converting salinity gradient power into electricity, compressed loofah-based RED showed good performance in terms of high power density and energy conversion efficiency.

Despite the good RED performances, desirable mechanical properties and dimensional stability in the aqueous solution are crucial to enhance the durability, which is favorable to reduce

costs of ISMs. After chemical modification, compression and epoxy resin-filling processes were used to fill the loofah pores and voids, which can improve the mechanical properties of the resultant ISMs. As shown in **Figure 7**a, the modified loofah
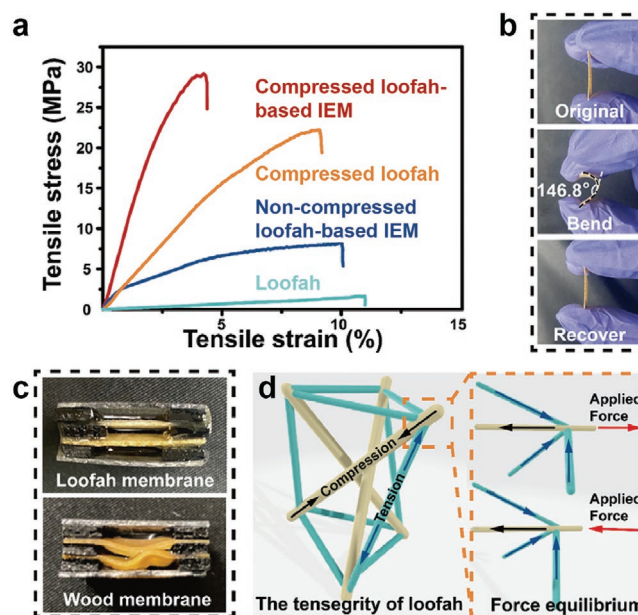

Figure 7. Characterization of mechanical properties and dimensional stability of loofah-based ISMs. a) Tensile strength of compressed loofah-based ISMs, compressed loofah, non-compressed loofah-based ISMs, and non-compressed loofah. b) The bendability photographs of compressed loofah-based ISM. c) The dimensional stability photographs of compressed loofah-based ISM (top) and the wood membrane (bottom). d) Schematic illustration of the tensegrity of the loofah.

ADVANCED
SCIENCE NEWS
www.advancedsciencenews.com

NANO · MICRO
small
www.small-journal.com

after compression and resin-filling (compressed ISMs) had a tensile strength of 29.1 MPa, which was 16.5 times higher than that of natural loofah and 3.6 times of non-compressed ISMs. Additionally, the compressed ISMs also showed good bendability, which can be bent to 146.8° and recovered to its original shape without damage and deforming (Figure 7b). Furthermore, membranes with a higher swelling degree are normally easier to deform in an aqueous solution, especially for thin membranes.[20] But the compressed ISMs still showed excellent dimensional stability after soaking in the NaCl solution for three months (Figure S10, Supporting Information), although it had a high swelling degree. However, home-made wood membranes with lower swelling degrees underwent severe deformation under the same conditions (Figure 7c). Moreover, the wet compressed ISMs also exhibited a tensile strength as high as 7.7 MPa (Figure S11, Supporting Information). The good mechanical performance and dimensional stability of our ISMs can be attributed to its sponge isotropic structures of loofah, which followed the tensegrity principle. Figure 7d showed that the typical tensegrity structure maintained its shape by the equilibrium between the opposing forces of tension and compression and the applied forces. In contrast, other lignocellulosic biomass-based heterogeneous ISMs normally exhibited a nonuniform anisotropic microstructure. When exerting external forces or swelling, these biomass were easier to deform or break than loofah-based ISMs. Good mechanical strength under both wet and dry states and excellent dimensional stability enabled compressed loofah-based ISMs a great potential in large-scale application and long-time use in the RED.

3. Conclusion

The high price of ISMs and relatively low power density are major obstacles for large-scale salinity gradient power harvesting. In this work, for the first time, we have fabricated loofah-based ASMs and CSMs for affordable and high-performance RED through chemical modification, compression, resin filling, and polishing. The as-prepared loofah-based ISMs exhibited desirable mechanical properties, bendability, dimensional stability, high ion conductivity, and high permselectivity owing to unique 3D interconnected multichannel structures, high water absorption, and excellent compressibility. The ion conductivity and permselectivity of the resultant loofah-based ISMs strongly depend on their fiber and charge density. The compressed loofah-based ISMs exhibited excellent permselectivity (96.8%) at the concentration gradients of 60 and ion conductivity at a low salt concentration (0.543 mS cm^{-1} for CSM and 0.620 mS cm^{-1} for ASM after soaking in 0.001 M NaCl solution for 24 h). As a result, the maximum output power density of a RED unit assembled with compressed loofah-based CSM and ASM was 18.3 mW m^{-2} under the concentration gradient of 60. The 10 tandem RED units were able to generate up to 1.55 V of output voltage. The loofah-based ISMs derived from natural low-cost loofah sponge with natural-derived multichannels, high hydrophilicity, and excellent processability, pave the way to design and fabricate affordable, durable, and high-performance ISMs for salinity gradient power generation.

4. Experimental Section

Materials: Natural loofah sponge and Basswood were purchased from SHANGHAI BILANTENG Net Co., ltd and BeaverCraft Inc. (3-Chloro-2-hydroxypropyl) Trimethylammonium Chloride (CHPTAC, 65 wt.%) and Sodium hydroxide (NaOH) were purchased from Fisher Scientific. 2,2,6,6-Tetramethylpiperidine 1-oxy radical (Tempo, 98%), Sodium bromide (NaBr), Cobalt chloride (CoCl$_2$ · 2H$_2$O), Nile Red (C$_{20}$H$_{18}$N$_2$O$_2$), and Sodium hypochlorite (NaClO, 10–15%) were purchased from Sigma-Aldrich. 300/21 Epoxy resin was purchased from Aeromarine Products Inc. Deionized water was used in the whole study.

Material Preparation: Loofah was first prepared by removing the core portion of natural loofah sponge and cutting it into three pieces (Figure S1a, Supporting Information).

Cationic Modification of Loofah: P-loofah was prepared through etherification and quaternization with CHPTAC. 10 g of loofah was preheated at 85 °C in 300 mL water for 0.5 h and then 18 g of NaOH was added to the solution and kept at 85 °C for 4 h. The resulted loofah was washed several times by water and then immersed into 300 mL water at 60 °C for 0.5 h. 26.7 g of NaOH was added to the solution and kept at 85 °C for another 0.5 h. Then, 80g of CHPTAC was added dropwise into the solution. The reaction was finished after 4 h. The resulted P-loofah was washed with water several times and stored in ethanol solution.

Anionic Modification of Loofah: N-loofah was prepared through TEMPO-mediated oxidation. 10g of loofah was immersed in water (800 mL) containing TEMPO (0.2 g) and NaBr (1.5 g). Then, 10 mmol of NaClO was added dropwise into the solution at room temperature while maintaining the pH 10.5 by adding 0.5 mol L^{-1} NaOH solution. The reaction was finished by 10 mL of ethanol when the pH of the solution stayed unchanged. The resulted N-loofah was washed with water several times and stored in ethanol solution.

Preparation of the Loofah Membranes: The P- and N-loofah were first taken out from the ethanol solution and hot pressed at 60 °C for 30 min and 10 h to get a medium compressed and fully compressed structure. After compression, the pore volume of fully compressed loofah and medium compressed loofah was reduced by 88% (0.48 cm^3 g^{-1}) and 42% (2.28 cm^3 g^{-1}), respectively. The medium compressed and fully compressed loofah were then immersed in the mixed solution of the epoxy resin and curing agent at a weight ratio of 2:1 and then transferred into a vacuum desiccator at room temperature to remove the gas in the film. The vacuum condition was lasted for approximately 5 min and then returned to atmospheric pressure to allow the resin into the loofah structure. This process was repeated 3 times in 30 min. Subsequently, the filled films were stored in the atmosphere for 24 h to ensure complete solidification. Finally, the film was polished to get a uniform thickness of 0.3 mm and cut into pieces (2 × 2 cm).

Preparation of the RED: The RED was consisted of alternating ASMs and CSMs with an effective area of 0.6 cm^2 and separating by rubber sheets with a thickness of 1.5 mm (Figure S8a–c, Supporting Information).

Characterization Methods: The morphology of loofah was characterized by scanning electron microscopy (SEM, Hitachi S4800, Hitachi Ltd., Japan) and optical microscopy (Stereo Discovery. V12, Carl Zeiss, Germany). FTIR was conducted using a Nicolet 5700 spectrometer (Bruker Corp., USA).

The morphology of loofah-based ISM was characterized by laser scanning confocal microscopy (LSCM, Leica TCS SP8, Leica Microsystems, Germany) with a Z-slice step size of 0.2 µm/slice increments at 510 nm. The loofah fiber after anionic or cationic modification was first dyed by Nile Red at room temperature for 24h and then filled resin and polished.

The pore diameter distribution was carried out by a Micromeritics ASAP 2460 volumetric adsorption analyzer at 77 K (ASAP 2460, Micromeritics, USA). The pore size was calculated by using Barrett–Joyner–Halenda (BJH) formula.

The water adsorption was measured by immersing dried samples into the water at vacuum at 20 °C for 1 h, and then transferred to atmospheric pressure for 24 h. Afterwards, the wet sample was wiped

ADVANCED
SCIENCE NEWS

www.advancedsciencenews.com

NANO · MICRO

small

www.small-journal.com

by filter paper to remove extra water and weighed quickly. The water adsorption was calculated as follows:[36]

$$\text{Water adsorption} = \frac{w_1 - w_0}{w_0} \tag{1}$$

Where w_0 is the weight of dried sample and w_1 is the weight of wet sample.

The zeta potential tests of loofah, P-loofah, and N-loofah were determined three times using a Nano ZS Zetasizer (Malvern Instruments, Worcestershire, UK). Before zeta potential tests, the loofahs were first ball milled to powder, then diluted to 0.1 mg mL^{-1} by different solutions (deionized water, 0.001 M NaCl, 0.01 M NaCl, and 0.1 M NaCl), and sonicated for 12 h. Besides, the zeta potential tests at different pH were performed in 0.1 M NaCl solutions adjusted by 0.5 mol L^{-1} NaOH and HCl solutions.

Based on the zeta potential results, the surface charge density was calculated by Grahame equation as:[37]

$$\sigma = \frac{\varepsilon \times \varepsilon_0 \times \zeta}{\lambda_d} \tag{2}$$

Where σ is the surface charge density, ε_0 is the vacuum permittivity (8.85419×10^{-12} C m^{-1} V^{-1}), ε is the dielectric permittivity (78.36) of water at 25 °C, and ζ is the zeta potential (mV), λ_d is the Dyebe length (nm).

The λ_d is calculated by the following equation:

$$\lambda_d = \frac{0.304 \text{ nm}}{\sqrt{c_0 \frac{L}{mol}}} \tag{3}$$

Where c_0 is the concentration of NaCl solution (mol L^{-1}).

Mechanical Tests: The tensile strength tests of the samples were conducted by a universal testing machine (Instron Model 5567) with a test speed of 10 mm min^{-1}. The dimensions of testing samples were approximately 15 mm by 3 mm by 0.3 mm. For wet samples, the samples were immersed in water for 8h and wiped with filter paper to remove excess water before testing.

The dimensional stability of the compressed loofah membrane and wood membrane were determined by immersing in 0.6 M NaCl solution at room temperature.

Electrochemical Performance Measurements: The EIS was conducted with a voltage amplitude of 5 mV over a frequency range from 100 kHz to 100 mHz. After immersing in the different NaCl concentrations, the samples were clamped by two Cu foils and tested. The membrane resistance can be read from the EIS and the ion conductivity was calculated as follows:

$$\sigma = \frac{d}{R \times A} \tag{4}$$

where σ is the ion conductivity of the membrane, d is the membrane thickness, R is the membrane resistance, and A is the effective area of the membrane.

The I-V curves of the built ion conductor were recorded by a Keithley Sourcemeter (Tektronix, USA) using Ag/AgCl plate as the electrode (Figure S9, Supporting Information). High concentration of NaCl solution was filled in the middle reservoir and low concentration NaCl solution (0.001 M) was in the side reservoir. Sweeping voltage was from −300 to 100 mV with an increasing voltage rate of 20 mV. The intersection of the I-V curves at the y-axis and the x-axis were read as the open-circuit voltage (U_{oc}) and the short-circuit current (I_{sc}). The RED performance under different pH conditions was carried out at high NaCl concentration of 0.1 M and low NaCl concentration of 0.001 M. Besides, in order to ensure that changing the pH will not greatly affect the salt concentration difference, only the high concentration of NaCl solution was adjusted by 0.5 mol L^{-1} NaOH and HCl solution.

The membrane permselectivity (α) and electrochemical energy conversion efficiency (η) were calculated as follows:[38,39]

$$\alpha = \frac{V_{meas}}{V_{theo}} \times 100\% \tag{5}$$

$$V_{theo} = 2N\frac{RT}{zF}\ln\frac{a_c}{a_d} \tag{6}$$

$$\eta_{maxW} = \frac{\alpha^2}{2} \times 100\% \tag{7}$$

where V_{meas} is the membrane potential got from I-V curves, V_{theo} is the theoretical membrane potential obtained from the Nernst equation, N is the number of membrane pairs; R is the gas constant (8.314 J (mol^{-1} K^{-1})), T is the absolute temperature (K), z is the electrochemical valence, F is the Faraday constant (96485 C mol^{-1}), a_c and a_d are the activity of concentrated and diluted NaCl solution (mol L^{-1}), and η_{maxW} corresponds to energy efficiency at the maximum power output.

The maximum power output (W_{max}) and maximum power density (w_{max}) were calculated as follows:[40]

$$W_{max} = \frac{U_{oc} \times I_{sc}}{4} \tag{8}$$

$$w_{max} = \frac{W_{max}}{NA} \tag{9}$$

Where U_{oc} is the open-circuit voltage, I_{sc} is the short-circuit current, N is the number of membrane pairs, and A is the effective membrane area.

Supporting Information

Supporting Information is available from the Wiley Online Library or from the author.

Conflict of Interest

The authors declare no conflict of interest.

Data Availability Statement

Research data are not shared.

Keywords

[1] IEA, *Global Energy Review. IEA*, Paris, France **2019**.
[2] A. Barreira, M. Patierno, C. R. Bautista, *Perspect* **2017**, *28*, 1.
[3] J. G. Olivier, K. Schure, J. Peters, *Trends in global CO₂ and total greenhouse gas emissions*, PBL Netherlands Environmental Assessment Agency, The Hague, NL **2017**.
[4] C. F. Kutscher, J. B. Milford, F. Kreith, *Principles of sustainable energy systems*, CRC Press, Boca Raton, FL **2018**.

ADVANCED
SCIENCE NEWS

www.advancedsciencenews.com

NANO · MICRO

small

www.small-journal.com

[5] J. W. Post, H. V. Hamelers, C. J. Buisman, *Environ. Sci. Technol.* **2008**, *42*, 5785.

[6] J. N. Weinstein, F. B. Leitz, *Science* **1976**, *191*, 557.

[7] G. L. Wick, W. R. Schmitt, *Mar. Technol. Soc. J.* **1977**, *11*, 16.

[8] J. D. Isaacs, R. J. Seymour, *Int. J. Environ. Stud.* **1973**, *4*, 201.

[9] G. Z. Ramon, B. J. Feinberg, E. M. Hoek, *Energy Environ. Sci.* **2011**, *4*, 4423.

[10] S. Loeb, F. V. Hessen, D. Shahaf, *J. Membr. Sci.* **1976**, *1*, 249.

[11] R. A. Rica, R. Ziano, D. Salerno, F. Mantegazza, R. V. Roij, D. Brogioli, *Entropy* **2013**, *15*, 1388.

[12] A. Siria, P. Poncharal, A. L. Biance, R. Fulcrand, X. Blase, S. T. Purcell, L. Bocquet, *Nature* **2013**, *494*, 455.

[13] Q. She, Y. K. W. Wong, S. Zhao, C. Y. Tang, *J. Membr. Sci.* **2013**, *428*, 181.

[14] W. R. Thelin, E. Sivertsen, T. Holt, G. Brekke, *J. Membr. Sci.* **2013**, *438*, 46.

[15] B. Zhang, H. Gao, X. Tong, S. Liu, L. Gan, Y. Chen, in *Current Trends and Future Developments on (Bio-) Membranes* (Eds: A. Basile, A. Cassano, A. Figoli), Elsevier, Amsterdam, NL **2019**, p. Ch. 6.

[16] T. Xu, *J. Membr. Sci.* **2005**, *263*, 1.

[17] Q. Y. Wu, C. Wang, R. Wang, C. Chen, J. Gao, J. Dai, D. Liu, Z. Lin, L. Hu, *Adv. Energy Mater.* **2020**, *10*, 1902590.

[18] J. Shen, Y. M. Xie, X. Huang, S. Zhou, D. Ruan, *Int. J. Impact Eng.* **2013**, *57*, 17.

[19] J. Shen, Y. M. Xie, X. Huang, S. Zhou, D. Ruan, *J. Mech. Behav. Biomed. Mater.* **2014**, *15*, 141.

[20] L. Zeng, Q. Liu, M. Lu, E. Liang, G. Wang, W. Xu, *Chem. Eng. Res. Des.* **2019**, *150*, 26.

[21] K. E. Bal, Y. Bal, A. Lallam, *Text. Res. J.* **2004**, *74*, 241.

[22] H. Demir, U. Atikler, D. Balköse, F. Tıhmınlıoğlu, *Composites, Part A* **2006**, *37*, 447.

[23] F. Wang, J. Dai, L. Huang, Y. Si, J. Yu, B. Ding, *ACS Nano* **2020**, *14*, 8975.

[24] I. Vlassiouk, S. Smirnov, Z. Siwy, *Nano Lett.* **2008**, *8*, 1978.

[25] J. Ji, Q. Kang, Y. Zhou, Y. Feng, X. Chen, J. Yuan, W. Guo, Y. Wei, L. Jiang, *Adv. Funct. Mater.* **2017**, *27*, 1603623.

[26] L. Cao, W. Guo, J. Xia, F. Q. Nie, W. Ma, J. Xue, Y. Song, D. Zhu, Y. Wang, L. Jiang, *Adv. Funct. Mater.* **2010**, *20*, 1339.

[27] Y. Mei, C. Tang, *Desalination* **2018**, *425*, 156.

[28] R. C. Pettersen, *The chemical composition of wood*, ACS Publications, Washington, USA **1984**.

[29] A. Saeed, M. Iqbal, *Biotechnol. Prog.* **2013**, *29*, 573.

[30] S. Heiss-Blanquet, D. Zheng, N. L. Ferreira, C. Lapierre, S. Baumberger, *Bioresour. Technol.* **2011**, *102*, 5938.

[31] S. Poddar, M. Kamruzzaman, S. Sujan, M. Hossain, M. Jamal, M. Gafur, M. Khanam, *Fuel* **2014**, *131*, 43.

[32] A. Hashem, R. M. El-Shishtawy, *Adsorpt. Sci. Technol.* **2001**, *19*, 197.

[33] Y. Wang, L. Zhao, H. Peng, J. Wu, Z. Liu, X. Guo, E. Data, *J. Chem. Eng. Data.* **2016**, *61*, 3266.

[34] S. Fujisawa, Y. Okita, H. Fukuzumi, T. Saito, A. Isogai, *Carbohydr. Polym.* **2011**, *84*, 579.

[35] C. Liu, K. Hong, X. Sun, A. Natan, P. Luan, Y. Yang, H. Zhu, *J. Mater. Chem. A* **2020**, *8*, 12323.

[36] Q. Wu, L. Wan, Z. Xu, *J. Membr. Sci.* **2012**, *409*, 355.

[37] H. J. Butt, K. Graf, M. Kappl, *Physics and Chemistry of Interfaces*, Wiley, Hoboken, NJ **2003**.

[38] D. Kim, C. Duan, Y. Chen, A. Majumdar, *Microfluid. Nanofluid.* **2010**, *9*, 1215.

[39] E. Güler, R. Elizen, D. A. Vermaas, M. Saakes, K. Nijmeijer, *J. Membr. Sci.* **2013**, *446*, 266.

[40] P. Długołęcki, K. Nymeijer, S. Metz, M. Wessling, *J. Membr. Sci.* **2008**, *319*, 214.